Thermal lens Z-scan measurements for the determination of fluorescence quantum yields: theoretical and experimental uncertainties for low and high quantum yields

Georges Boudebs, Julien-Bilal Zinoune, Christophe Cassagne, Mihaela Chis

This article has been published in Applied Optics.

Get Citation:

Georges Boudebs, Julien-Bilal Zinoune, Christophe Cassagne, and Mihaela Chis, "Thermal lens Z-scan measurements: theoretical and experimental uncertainties for low and high fluorescence quantum yields," Appl. Opt. **62**, 7669-7677 (2023).

https://doi.org/10.1364/AO.500526

Accepted author version.

Thermal lens Z-scan measurements for the determination of fluorescence quantum yields: theoretical and experimental uncertainties for low and high quantum yields

GEORGES BOUDEBS,[1,*] JULIEN-BILAL ZINOUNE,[1,2] CHRISTOPHE CASSAGNE,[1] AND MIHAELA CHIS[1,2]

[1]*Univ Angers, LPHIA, SFR MATRIX, F-49000 Angers, France*
[2]*ESAIP, CERADE, 18, rue du 8 mai 1945, 49180 St-Barthélemy d'Anjou Cedex, France*
**georges.boudebs@univ-angers.fr*

Abstract: The single-beam Z-scan thermal lens (TL) technique is conducted to evaluate the fluorescence quantum yield of various solutions in the case of high-moderate absorption. Considering both scenarios: solutions with substantial fluorescence and solutions with high thermal efficiency but low fluorescence. An analytical calculation is performed to determine the uncertainties associated to the random errors introduced by optical detectors. The results reveal that solutions with low fluorescence led to a significant error, whereas higher fluorescence can help decreasing the uncertainty. Additionally, the issue of random errors arising when multiple measurements are needed to accurately estimate the fluorescence of a solution will be discussed in different situations.

1. Introduction

Thermal lens measurement techniques encompass a broad spectrum of applications, with a notable focus on calorimetry and spectroscopy. These techniques have been extensively employed in a multitude of studies aimed at precisely characterizing the thermal [1, 2, 3] and optical [4, 5, 6] properties of various compounds and materials. One of the first was the measurement of small absorption in low-loss liquids and solids as low as $10^{-5}\ cm^{-1}$ [7] showing that it can serve as highly sensitive absorption spectrometers especially using pumb-probe mode mismatched measurements [8, 9]. On the other hand, the single-beam Z-scan method has often been used with pulsed lasers for third-order nonlinear susceptibility measurements (see for example [10, 11, 12]) distinguishing between the real and imaginary parts of this physical quantity. Basically, these two methods are based on the far field diffraction phenomenon and are designed and known to measure relatively small, induced phase shifts with a sensitivity of a few tens of mrad at room temperature [13]. The combination of these two techniques should give even greater robustness to the so-called Z-scan TL based measurements which will be considered here. In their significant contribution, Hu and Whinnery [14] highlighted an additional use of thermal lensing measurement, which can be combined with conventional transmission data to calculate the fluorescence quantum yield. Initially, the total power absorbed by the dye solution is determined through energy transmission measurement. Subsequently, the power converted into heat is measured using the TL method. The difference between these two measurements is assumed to represent the power that has been emitted through fluorescence. This constitutes an indirect yet absolute method for measuring fluorescence. Several techniques are available for fluorescence measurements [15, 16, 17], with the most widely used one being the spectrofluorometer. Initially conceived by Vavilov [18] and subsequently refined by Parker et al. [19], the spectrofluorometer performs direct measurements relative to a known standard sample. The diversity of techniques and protocols has, in turn, led to variations in outcomes when applied to the same species [16, 20, 21]. The determination of the absolute value of fluorescence

quantum efficiency has been proven to be challenging, leading to conflicting results in the literature. While pure optical techniques can be employed to determine quantum efficiency, calibration is often problematic. The Z-scan technique relies on the absorption of light by the sample to generate a TL effect. If the sample has low extinction absorption, the sensitivity of the measurement decreases, making it challenging to accurately measure fluorescence signals [22]. On the other hand, if absorption is increased, mathematical formulas using the TL technique assume a first-order expansion of Beer-Lambert-Bouguer's law, and results derived from this approximation become unreliable.

Recently, experimental determination of the absorption and scattering efficiencies of spherical gold nanoparticles (NPs) with different diameters was carried out using the TL effect at three distinct wavelengths: blue, green, and red. The measurement method's key features, including the experimental procedure for weak absorption using Gaussian beams and its extension to higher absorption with top-hat beams, are thoroughly explained to provide a comprehensive understanding. In order to validate our approach, the obtained experimental TL data was compared to the theoretical values derived from Mie theory. Remarkably, the comparison showed a high level of agreement, within the limitations of experimental errors [23].

It would nevertheless be useful to recall the advantages and disadvantages of the Z-scan TL method, which we have frequently used for third-order nonlinear optical measurements. It is indeed a valuable technique for fluorescence measurement in certain situations. This method offers high sensitivity, and it can detect very low levels of fluorescence signals. One of the key advantages is its ability to suppress background noise effectively. By detecting the signal in the far field ($2\ m$ away from the cell) with a small-aperture PD, there is very little risk of detecting signals from scattering and fluorescence diffused in all directions around the focal spot-line, while only thermal effect optical signals propagate axially through a very small solid angle to reach the detector. This enables precise measurement of the desired fluorescence signal without significant background contamination. The TL method is a gentle, generally non-destructive method. It does not alter or damage the sample during measurement using relatively moderate power, making it suitable for analyzing delicate or valuable samples in thin films [24] or those having two photon absorption [25]. Z-scan TL can provide high spatial resolution in fluorescence measurements. By focusing the laser beam to a small spot, it allows for localized analysis, enabling to investigate specific regions or features within the solution and obtain detailed information about their fluorescence properties. So, Z-scan TL qualitative imaging method can be applied to various types of samples as in thin films [26], inhomogeneous solid surfaces [11, 27], and even biological tissues [28]. This versatility makes it a useful tool in many fields, such as environmental monitoring, pharmaceutical analysis, and bioimaging but one need to take more parameters into account than those considered so far. It could be combined with a phase object to differentiate the various phenomena that can occur in light-matter interaction as it has been done in [29]. In many cases, the TL method requires minimal sample preparation. It can directly analyze samples without the need for complex labeling or immobilization procedures, saving time and resources. It can provide information about the fluorescence lifetime of a sample. By analyzing the TL decay curve, it is possible to extract valuable kinetic and dynamic information, which can be useful for studying molecular interactions, photochemical processes, and other time-dependent phenomena. Moreover, in terms of microscopic dimensional metrology, incorporating doping fluorescent nanoparticles could serve as a viable solution for specific measurement-problem types [30].

However, Z-scan TL efficiency depends on various factors and limitations of the method in relation to the particular application at hand. Measuring the fluorescence of a solution has certain disadvantages. It relies on the absorption of light by the sample to generate a TL effect. If the sample has low extinction coefficient, the sensitivity of the measurement decreases, making it challenging to accurately measure fluorescence signals having even

more lower absorption TL coefficients. It is not well-suited for measuring the fluorescence of solutions throughout their entire volume, thickness must be less than the Rayleigh range of the incident beam. So, the TL effect is limited in depth profiling capabilities. Interpreting the Z-scan TL data can be complex, especially when dealing with samples that have complex optical properties or heterogeneous compositions. The analysis often requires sophisticated mathematical models and assumptions, which can introduce uncertainties in the measurement. Moreover, this technique, sometimes, involves focusing a high-intensity laser beam onto the sample, which can lead to photothermal damage [31], particularly in sensitive samples or those prone to photochemical reactions. This can alter the fluorescence properties, affecting the accuracy and reliability of the measurements. Z-scan experiments typically involve multiple measurements. The Z-scanning process can be time-consuming, especially when trying to obtain a reliable and statistically significant dataset. In addition, the accuracy of Z-scan TL measurements is highly dependent on the stability of the laser source which is another parameter which will not be considered here. Any fluctuations or instabilities in the laser power or beam profile can introduce errors or noise into the measurements, affecting the precision and reproducibility of the results.

In this paper, we will present the argument that the single beam Z-scan TL method is not just an alternative approach to measuring fluorescence quantum yields, but rather offers substantial advantages provided that the appropriate measurement errors are taken into account [32, 33, 34]. To achieve this, we will extend the application of this method to solutions with relatively higher absorbance. We will conduct measurements across various compounds, ranging from low to high fluorescence yields. Afterwards, this paper aims to examine the potential sources of errors that may arise and their impact on the measurement of fluorescence quantum yield. We are only interested in the error generated by the photodetectors, bearing in mind that there are other errors that can also influence the final result of the absolute measurement relative to the fluorescence quantum yield. Relative methods, however, yield the highest accuracy. To address this, it might be reasonable to create customized standards tailored to specific requirements. For instance, one could employ the TL method to measure very low fluorescent sample and promptly compare it to the current unknown of interest.

Our findings in this paper clearly demonstrate that the measurements uncertainties are not constant as is often considered in the literature but variable, increasing rapidly as quantum yield decreases. The number of measurements for low yields must therefore be increased to compensate for the higher relative error.

2. Theory

The theory relies on the concept of thermal lensing, which arises from localized variations in the optical index caused by the temperature distribution resulting from the absorption of light, specifically in our case, a single Gaussian laser beam. Let us start by distinguishing and clearly defining the two coefficients needed to measure the fluorescence efficiency (hereafter denoted as Φ). The absorption coefficient α_a, expressed in units of inverse length (e.g., in m^{-1}), is a measure of the material's ability to absorb photons of specific energy levels. It is defined according to the Beer-Lambert-Bouguer law relating the optical attenuation in a solution to the path length L. The intensity change in the laser light as it passes the absorbing medium is expressed by: $\Delta I(r) = I_0(r)\big(1 - exp(-\alpha_a L)\big)$ with $I_0(r)$ being the radial intensity profile at the entry. The extinction coefficient α_e is theoretically defined using the same law by measuring the transmitted power through two identical cells using a first cell filled with pure solvent, and a second one filled with the tested solution (see Appendix 1). It is related to absorption and other energy-loss processes that occur when light interacts with the travelled medium. It characterizes the total reduction in light power due to absorption, scattering, fluorescence luminescence… It is assumed here that the incident energy is transformed only into heat or fluorescence. Other losses are considered negligible.

The following symbols will be used: ρ density in Kg/m^3; I beam intensity in W/m^2; L thickness of the medium (cell) in m; P beam power in W (taking into account the Fresnel reflection); c specific heat in $J/Kg/K$; ω beam radius in m; ΔT temperature variation in°K; k thermal conductivity in $J/s/m/K$; λ wavelength in m. The usual TL approximations are assumed following references [23, 35, 36]: i) thin sample; ii) beam-waist considered small when compared to the dimensions of the cell. An expression of the temperature change as a function of radius r and time $\Delta T(r,t)$ can be obtained by solving the non-steady state heat equation with a Gaussian beam illuminating the medium [23, 37]:

$$\Delta T(z,r,t) = \frac{2P\alpha_{eff}}{\pi c\rho\omega^2(z)} \int_0^t \left(\frac{1}{1+2t'/t_c}\right) exp\left(\frac{-2r^2/\omega^2(z)}{1+2t'/t_c}\right) dt', \quad (1)$$

where $\alpha_{eff} = (1 - e^{-\alpha_a L})/L$ and $t_c(z) = c\rho\omega^2(z)/4k$ is the characteristic buildup time constant.

Note that in the special case where $\alpha_a L \ll 1$, we come back to the approximation used in [36] ($\Delta I(r) = I_0(r)\alpha_a L$) but for the more general case with relatively larger absorbance (while remaining with $\alpha_a L < 1$), α_{eff} should be considered. Here, α_{eff} could replace the absorption in the derived equations of Sheldon et al. [36] to define the phase lag characteristic quantity θ_{eff} relative to α_{eff} :

$$\theta_{eff} = \frac{PLdn/dT}{\lambda k}\alpha_{eff} = \frac{Pdn/dT}{\lambda k}[1 - exp(-\alpha_a L)], \quad (2)$$

with dn/dT denoting the algebraic value of the thermo-optical coefficient.

The change in the linear index due to this temperature variation is:

$$\Delta n(z,r,t) = \frac{dn}{dT}\Delta T(z,r,t), \quad (3)$$

with $\Delta n(z,r,t) = n(z,r,t) - n_0$ where n_0 is the refractive index at the initial temperature. The phase shift is related to Δn as usual, using $\Delta\varphi = 2\pi\Delta nL/\lambda$. The single-beam configuration that we consider here states that the beam induces $\Delta\varphi$ and probes it at the same time.

3. Principle of the optical method

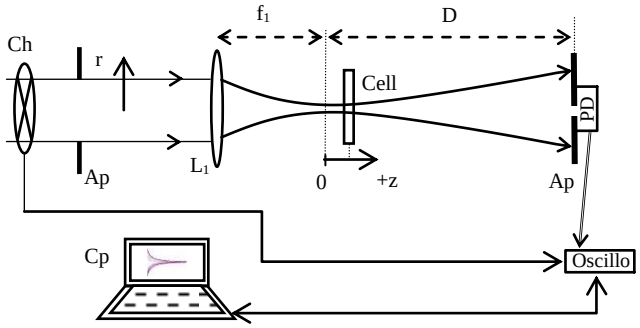

Fig. 1: Scheme showing the different position of the optical elements. The cell is scanned along the beam direction around the focal plane (z=0). The labels refer to: lens (L_1), chopper (Ch), circular aperture (Ap), computer (Cp) and photodiode (PD).

The principle of the single beam method, which is now well known, has already been explained in detail in [23, 35]. For self-consistency, we summarize here the most significant features of the technique. The setup (Fig. 1) has the advantage of combining a Z-scan configuration when the sample moves along z (focal region of lens L_1) and a TL signal describing the time response profile when the chopper rotates for each position z. The signal is obtained on a photodiode (PD) that acquires the central variation of the diffracted far field beam intensity versus z, the position of the specimen. This is equivalent to performing what is commonly referred to as a "closed aperture Z-scan". The PD is connected to a digital storage

oscilloscope where the signal S is only revealed by a TL effect in the cell which allows the measurement of α_a. S is defined as the fractional change in intensity when the cell is located at z after reaching the steady state regime as t approaching infinity:

$$S(z) = \frac{[I(z,t=0)-I(z,\infty)]}{I(z,\infty)}. \quad (4)$$

The analytical calculations presented in [35] yield the far field intensity variation at $r = 0$:

$$S(V) = C_{cal}\left[-1 + \frac{1}{1-\theta_{eff}tan^{-1}\left(\frac{2V}{3+V^2}\right)}\right] \quad (5)$$

where $V = z/Z_0$ with the Rayleigh distance $Z_0 = \pi\omega_{0f}^2/\lambda$ and ω_{0f} being the focused beam-waist at $z = 0$ (the focus of lens L_1). C_{cal} is a calibration factor that needs to be adjusted for each experiment, as it may depend on the shape of the input beam, which is not perfectly Gaussian, and all the experimental imperfections that could be encountered. This factor could be used as well when considering a reference solution with a specific characteristic. Eq. *(5)* allows to obtain θ_{eff} by fitting the experimental data. Following relationship (2), one can then find α_a, *i.e.*, the light truly absorbed in the medium:

$$\alpha_a = \frac{1}{L} ln\left[\frac{Pdn/dT}{Pdn/dT-\lambda k\theta_{eff}}\right]. \quad (6)$$

In contrast, the specimen's average extinction coefficient value α_e is determined by using an optical power meter (OPM) (Ophir, PD300UV, $10x10\,mm$ aperture [38]). This measurement is conducted by repeatedly varying the incident power and performing multiple measurements: $\alpha_e = ln(P_0/P_C)/L$ with P_0 being the transmitted power by the pure solvent and P_C the transmitted one by the solution that will be used in the experiment. The latter equation is employed to consider the Fresnel reflection that occurs between two identical cells.

Let Φ represent the ratio between the number of fluorescent photons to that of extinguished ones. It is assumed that the incident energy is transformed only into heat or fluorescence. Other losses are considered negligible: scattering, luminescence or other photoinduced light phenomena which spread out in the solution. This results in the determination of the light fluorescence efficiency Φ in relation to the overall light extinction, as calculated using the following equation (refer to the calculation details in Appendix A of reference [23]):

$$\Phi = \frac{\nu_i}{\langle\nu_f\rangle}\left[\frac{exp(-\alpha_a L)-exp(-\alpha_e L)}{[1-exp(-\alpha_e L)]}\right], \quad (7)$$

with ν_i and $\langle\nu_f\rangle$ representing the respective frequencies of incident photons and the average frequency of the emitted fluorescence. Note two points: i) this relationship reduces to a simpler expression, used up to now, if we consider the limiting case with low absorbances: $\Phi \approx \nu_i\left(1-\frac{\alpha_a}{\alpha_e}\right)/\langle\nu_f\rangle$; ii) $(1-\Phi)$ represents the portion of light extinction that is absorbed by the solutions, resulting in photothermal heating and the detection of the TL signal.

4. Experimental results

The room temperature was consistently maintained at 21°C throughout all the measurements. The study has been performed using cw laser at 532 nm with methanol-based solutions. The output laser beam was spatially filtered before collimation and truncated by a circular aperture resulting in a "top hat" beam of diameter $\approx 1.9\,mm$. It was then focused into the quartz cell (Thorlabs, CV10Q35) containing the solutions to be tested. The rotation of the two-bladed chopper was set at a frequency of $2\,Hz$ which gives $250\,ms$ of opening time

during which the solution is irradiated and $250\ ms$ of obstruction allowing the liquid to cool down between two acquisitions. These exposure times provide a sufficient duration for the temporal evolution to reach the nearly stationary regime. Typically, with $\omega_{0f} = 45\ \mu m$, the thermal response time of the methanol solvent is characterized by $t_c = c\rho\left(\omega_{0f}\right)^2/4k \approx 5.4\ ms$. This time can be regarded as very small when compared to the opening duration of the chopper. The scan on z is performed in the interval $-2 < V < 2$ so that $t_c(z)$ remains at most 10 times smaller than the opening time: $t_c(2Z_0) < 25\ ms$.

As an illustration, an experimental result is provided here using the $532\ nm$ laser with a solution of Rhodamine B (RhB), purchased from [39], and taking into account $C_{cal} = 1$. The blue stars experimental data in Fig. 2 ($S(V)$) are calculated using *Eq. (4)* and show a characteristic valley-peak profile. They are numerically processed to be symmetrical with respect to $V = 0$. Using *Eq. (5)*, the fitting of $S(V)$ allows to estimate the beam-waist of the focusing beam corresponding to a Rayleigh distance of $Z_0 = 1.22\ cm$ using a focal lens $f_1 = 25\ cm$. The thickness of the cell $L = 1\ cm$ is therefore compatible to be considered as a thin sample. Note that the incident power (inside the liquid) in this example was $P = 0.52\ mW$ resulting in a central peak intensity in the focus at $z = 0$, $I_0 = 0.16\ MW/m^2$.

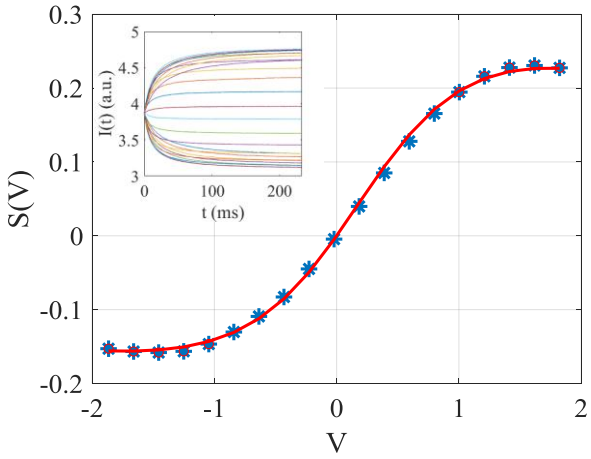

Fig. 2: Fitting (red solid line) of the Z-scan profile (blue stars) versus the normalized position V allowing to obtain θ_{eff}. The inset shows the temporal response at the PD.

The solid red line in Fig. 2 shows the fitting of the experimental data (blue stars) giving $\theta_{eff} = -353\ mrad$ with a solution having an overall extinction coefficient $\alpha_e = 49.95\ m^{-1}$ measured in a standard light transmission experiment via the OPM. Knowing $L = 1\ cm$, $dn/dT = -3.9 \times 10^{-4} K^{-1}$ and $k = 0.19\ J/s/m/K$ for methanol, the value of the TL absorption can be obtained from *Eq. (6)* giving $\alpha_a = 19.4\ m^{-1}$ and therefore the value of $\alpha_{eff} = 17.7\ m^{-1}$. Finally, according to *Eq. (7)* and considering the average emission photon energy ($2.1217\ eV$) for RhB [40], the measured fluorescence yield is $\Phi = 60.5\%$.

It is important to evaluate measurement error. Excessive measurement error compromises the validity and reliability of the results, necessitating careful assessment and mitigation strategies. Measurement error is categorized into two main types: random error and systematic error. Random error, generally defined as precision, focuses on the reproducibility and consistency of measurements; it occurs by chance and leads to slightly different results when measuring the same item multiple times, even if all steps are performed correctly. On the other hand, systematic error which is connected to accuracy focuses on how close those measurements are to the true or target value. It arises when the measurement system

consistently makes the same type of mistake, often due to issues with the measuring tool. Considering the accurate determination of the real power entering the sample is crucial as it directly impacts the measurement of α_a, α_e then Φ. Ideally, both high precision and high accuracy are required in a measurement system. In our case, to determine Φ, we must perform measurements on α_a and α_e. The assessment of α_e exclusively relies on the OPM, which introduces a total error, as indicated by the OPM data sheet [38, 41], with an accuracy of ±3% considering expanded error within 2.0 standard deviations with 95% confidence level. On the other hand, the measurement of α_a entails the utilization of both the OPM and the photodetector PD, resulting in a measurement error that is predominantly random in nature. Consequently, our statistical evaluation yields a total error, which is a composite of systematic and random errors. This error is referred to as a relative error throughout the following text. The mathematical details of the absolute random error calculation are reported to the Appendix 1:

$$\Delta\Phi = \frac{1}{\left(1-e^{-\alpha_e L}\right)}\sqrt{\left[e^{-\alpha_a L}\frac{\lambda k}{(P dn/dT-\lambda k\theta)}\sqrt{\left(-\frac{\theta}{P}\Delta P\right)^2+(\Delta\theta)^2}\right]^2+\left[e^{-\alpha_e L}\frac{\left(1-e^{-\alpha_a L}\right)}{\left(1-e^{-\alpha_e L}\right)}\sqrt{\left(\frac{\Delta P_0}{P_0}\right)^2+\left(\frac{\Delta P_C}{P_C}\right)^2}\right]^2} \quad (8)$$

where, to lighten the notation, we designed by θ the characteristic phase parameter θ_{eff} defined in *Eq. (2)*. Based on this last equation, a simulation program has been developed to find the variation of $\Delta\Phi/\Phi$ as a function of Φ taking into account the following experimental conditions:

1- Knowing $\lambda = 532\ nm, L = 1\ cm$, $dn/dT = -3.9\times10^{-4}K^{-1}$ and $k = 0.19\ J/s/m/°K$ for methanol with $\nu_i/\langle\nu_f\rangle = 1$.

2- Maintaining the linearity of $P(\theta)$ with a good signal-to-noise ratio: $0.1 < |\theta| < 0.4$ [23]. So, having the highest signal at the PD corresponds to $|\theta| \approx 0.3$ or 0.4.

3- Knowing that $\Delta\alpha_e = \frac{0.03\sqrt{2}}{L} = 4.2\ m^{-1}$ (see Appendix 1) relative to our OPM, we need $\alpha_e \gg \Delta\alpha_e$ to decrease the relative error with $(\alpha_e L)_{max} \lesssim 1$ (conditions for moderate absorptions) which requires $\alpha_e \approx 100\ m^{-1}$.

4- The simulation program therefore consists of varying Φ for a given α_e which allows to find α_a through Eq. (7). α_a allows to find P with $|\theta| = 0.4$ from Eq. (6). The obtained α_a for the varying Φ allows to calculate ΔΦ (Eq. 3) and therefore $\Delta\Phi/\Phi$ by taking the ratio.

The results of the numerical calculation are shown in Fig. 3. The coordinates of the point that appear on this figure demonstrate that when the yield Φ is less than 9%, the relative error on the measurement exceeds 100%. Moreover, Fig. 3 shows that in particular, the error will be less than 40% and therefore acceptable when Φ is greater than 20%. For lower Φ, this indicates that the measurement ceases to provide accurate and consistent results, making it uncertain and untrustworthy. This result could have been obtained more quickly by noting that Φ tends towards 0, forcing the $\Delta\Phi/\Phi$ ratio, of course, to tend towards infinity. But here significant values are obtained when Φ is large. For example, the relative error tends to cancel out when Φ tends towards 1, allowing to have lower relative errors on the quantum yield than those considered for the estimation of the incident power P and the diffracted signal through θ.

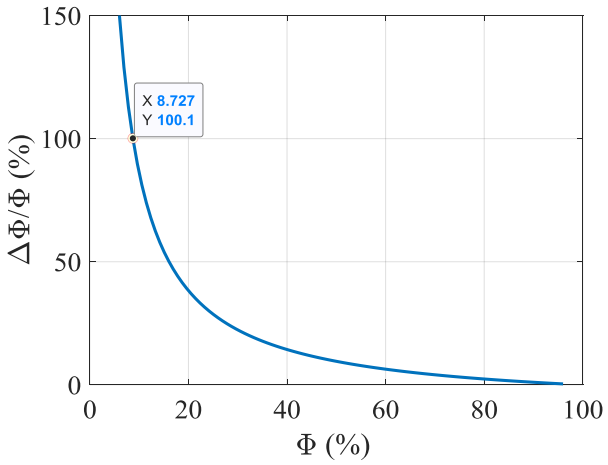

Fig. 3: Simulation of the relative error when measuring quantum yield as a function of Φ under the best experimental conditions given by our measuring instruments.

It would be interesting to determine the most crucial parameter that requires meticulous measurement considering the experimental used value of $|\theta| \approx 300\, mrad$ which is the approximate value used for assessing various fluorescent compounds hereafter. In fine, there are two parameters that we quantify with a silicon detector, the 1st on the OPM to measure power P and the 2nd on the PD to measure θ. Two simulations were carried out, the first dividing the relative error on θ by 10 and the second dividing the error on P by 10. The following Fig. 4 shows the two results in comparison with that given by the standard errors shown in blue solid line (3% with the OPM and 12% with the PD).

In Fig.4, the simulation reveals that the primary source of critical error for low values of Φ comes from the photodetector (PD). To minimize the overall measurement error, it becomes necessary to effectively decrease the PD error. Specifically, when measuring $|\theta| = 0.3$ with a range of $\Delta\theta = 35\, mrad$, the relative error exhibits 12%. Even with a PD that produces measurements with only a 1.2% error (as depicted by the green curve), it would be unrealistic to expect reliable measurement of a quantum yield below 10% with such high relative errors. Of course, by increasing the number of measurements, errors can be reduced.

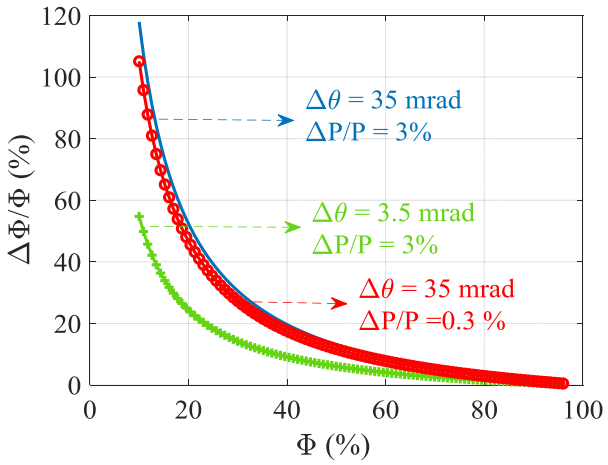

Fig. 4: Simulation of relative error of the quantum yield as a function of Φ. In blue solid line with the standard errors of the experiment. In red (o) by dividing the relative error on P by 10 and in green (+) by dividing the relative error on θ by 10.

Given the trend in uncertainty shown in Figs. 3 and 4, it seems obvious that the number of measurements needs to be increased more and more as yield decreases. On the other hand, one might think that it would be possible to calibrate the system with known solutions such as Rh6G with a high quantum yield ($\Phi \approx 0.95$), in order to make reliable measurements with products presenting lower yields. In reality, the sensitivity of the measurement is very low when the yield is high: the absolute value of the curve slopes given in Figs. 3&4 decreases exponentially with increasing Φ. Then a dilemma presents itself: faced with the decision of either conducting measurements with heightened sensitivity but significant uncertainties or opting for lower uncertainty and sensitivity simultaneously. We opted for the 1st solution, increasing sensitivity but taking many measures to reduce uncertainty. Using hexaaquacobalt(II) nitrate [42], $[Co(OH_2)_6][NO_3]_2$ (CoN), as a reference with the lowest fluorescence efficiency, after a considerable number of measurements (68), a calibration coefficient of $C_{cal} = 0.8821$ was derived adjusting the mean value of Φ to be close to 0. Consequently, table 1 represents the average of the obtained quantum yield values of different solutions in this scenario while the detailed measurements according to *Eq. (2)* are given in the Appendix 2. Note that each value obtained from Z-scan profile represents a mean value based on fitting performed on approximately twenty positions of the sample along the z-axis (see Fig. 2). This should normally give a more reliable measurement than a single measurement taken with a given cell position proceeding with TL method alone by fitting the time evolution of the signal using Eq. (36) in [36]. In Table 1, we give at the first line the average value of the absorption coefficient due to the thermal effect of the pure solvent (methanol purchased from [43]) as an indication. Additionally, we verified that when the same power was applied, the empty quartz cell did not exhibit a Z-scan signature indicative of any absorption.

Table 1: The quantum yield measured by Z-scan TL method using CoN as a reference solution with $\Phi \approx 0$.

Reference: CoN			$\lambda = 532\ nm$	
Solution	N files	$\alpha_a \pm \Delta\alpha_a (m^{-1})$	$\nu_i/\langle\nu_f\rangle$	$\Phi \pm \Delta\Phi$ (%)
Methanol	4	0.52 ± 0.06		

$[Co(OH_2)_6][NO_3]_2$ (CoN)	68		1	0 ± 4
Pararosaniline base (Para)	11		1	5 ± 6
Rhodamine B (RhB)	69		1.1	48 ± 4
Cresyl violet perchlorate (cresylV)	15		1.18	56 ± 2
Rhodamine 6G (Rh6G)	12		1.06	94 ± 1

To better visualize the distribution of the quantum-yield relative to the different solutions, we have reproduced the results of the measurements shown in table 1 on Fig. 5(a) as a function of input power. For the two products where Φ is low (CoN and pararosaniline base [44]) measured values are much more dispersed than for the others, noting that in contrast, Rh6G values are well confined around 94% with very little variation.

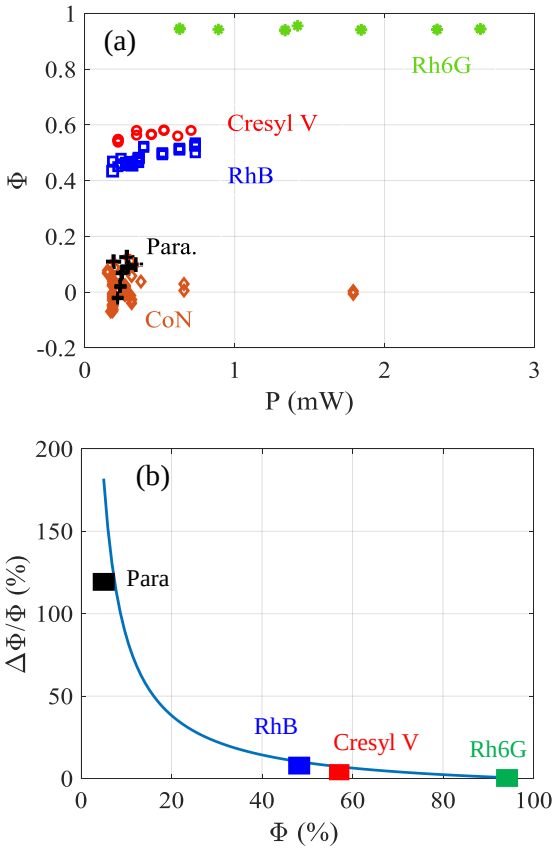

Fig. 5: (a) Distribution of Φ values for the different methanol-based solutions measured as a function of P. (b) Comparison of the experimental measurements (colored squares, results of table 1) with the theoretical calculations (solid line) already shown in Fig. 3.

In Fig. 5 (b), the dispersion of the relative error with the quantum yield can be seen more clearly. Indeed, a comparison of the experimental results is made with the theoretical one shown in Fig. 3. The colored rectangular dots are taken from the last column of table 1 by dividing ΔΦ by Φ obtained following the method detailed in Appendix 2. Note that the agreement is almost perfect from a qualitative point of view, with a rapid decrease in relative error describing the uncertainties as a function of the yield. Obviously, the point representing

the CoN with a zero Φ is not shown, as its value is indeterminate on y-axis since it tends towards infinity.

Comparison is done between our measurements and some measurements found in the literature. The measured value for cresyl violet perchlorate [45] ($\Phi = 56 \pm 2$, see table 1) compared with that obtained by Isak and Eyring [46] or Magde et al. [47] considering an average concentration of $6.8 \times 10^{-5}\, M$, gives us essentially the same value to within experimental errors, whether the solution is made in methanol or ethanol. Another solution where measurements converge towards a stable value reported by several authors [48, 49, 50, 51] around a quantum yield of 0.95 is rhodamine 6G that was obtained from sigma [52]. Despite the relatively high concentrations we have considered ($\alpha_e(m^{-1}) = 82 \pm 4$), the mean value obtained using our technique corroborate exactly the results already established in these references considering the limit of low concentration. One point that should be stressed here is that the relative error on the Φ measurements can be very low (as low as 1% when $\Phi \approx 0.95$, see measurements done in [50]), whereas silicon-based detectors have a much larger relative error on the measurement at room temperature. For moderate quantum yields, the value measured for rhodamine B here, $\Phi = 48 \pm 4$, shows very good agreement with the mean values obtained for the base and acid forms in [53] with $\Phi = 48 \pm 10\%$. As already seen, when dealing with low quantum yields, TL techniques lose their effectiveness. In such cases, it is preferable to be careful with measurements, even at a value as low as $\Phi = 0.25$ [54]. The result of our theoretical and experimental calculations in Fig. 5(b) shows why there are not many measured values in the literature for the last two products we tried to use as references. Besides, it should be noted that, according to our measurements, pararosaniline has a slightly higher fluorescence yield than CoN. This result has been confirmed qualitatively by the naked eye, where a faint yellowish fluorescent line delimits the axis of light propagation inside the $1\ cm$ cell filled with this solution.

To conclude this paragraph, it would nevertheless be useful to recall that single-beam Z-scan TL method offers high sensitivity, and it can detect very low levels of fluorescence signals but remains highly unreliable requiring a very large number of measurements for low values of the quantum yield. Measuring quantum yields with conventional OPM for values below 20% (if a threshold is to be set) is fraught with uncertainty. To mitigate this uncertainty, the fundamental approach would involve reducing $\Delta\theta$, which represents the uncertainty in the Z-scan signal measurement, and to use a more sensitive photodetector with improved resolution. Achieving this can be accomplished through cooling, a technique already employed in infrared spectroscopy. One could also consider using a thermoelectrically cooled CCD camera, using a Peltier cooler to maintain a lower temperature of the sensor, resulting in improved signal quality and sensitivity. Of course, this would come at a significantly higher cost.

5. Conclusions

In this study, we have expanded the utilization of the single-beam thermal lens Z-scan technique to measure the fluorescence quantum yield of solutions with moderately high absorption. We have formulated analytical expressions to assess the measurement errors, revealing that uncertainty rapidly increases as the quantum yield decreases. When quantum efficiency is below approximately 20%, it is advisable to conduct the measurement a significant number of times. Our experiments covered a range of compounds, spanning from those with low to high fluorescence yields, validating the trends observed in our analytical models. The single-beam thermal lens Z-scan technique offers several advantages, make it a valuable tool for investigating the fluorescence properties of solutions, provided that the inherent measurement errors associated with this technique are accurately estimated.

Funding. Univ Angers. Laboratoire de Photonique d'Angers (LPHIA, EA 4464). SFR MATRIX.

Acknowledgments. The authors are thankful to Dr. Martinus H. V. Werts and Matthieu Loumaigne for helpful discussions and for donating the basic solutes used to prepare the solutions.

Disclosures. The authors declare no conflicts of interest.

Data availability. Data underlying the results presented in this paper are not publicly available at this time but may be obtained from the authors upon reasonable request.

Appendix 1

Here, we derive the analytical details of the mathematical calculation to evaluate the precision estimating the total error on the fluorescence quantum yield taking into account all measured parameters: $\alpha_e \pm \Delta\alpha_e$, $P \pm \Delta P$ and $\theta \pm \Delta\theta$ to find $\Phi \pm \Delta\Phi$. Note that θ is defined by Eq. (2).

1) $\boldsymbol{\alpha_e \pm \Delta\alpha_e}$

This parameter is measured from 2 OPM measurements through two identical cells: P_0, using a first cell filled with pure solvent, and P_C, through a second cell filled with solution at concentration C.

$$\alpha_e = \frac{1}{L} Ln\left(\frac{P_0}{P_C}\right).$$

If we consider the error on L to be negligible, we get:

$$\Delta\alpha_e = \sqrt{\left(\frac{\partial\alpha_e}{\partial P_0}\Delta P_0\right)^2 + \left(\frac{\partial\alpha_e}{\partial P_C}\Delta P_C\right)^2}$$

Now, $\frac{\partial\alpha_e}{\partial P_0} = \frac{1}{LP_0}$ and $\frac{\partial\alpha_e}{\partial P_C} = -\frac{1}{LP_C}$ which results in:

$$\Delta\alpha_e = \frac{1}{L}\sqrt{\left(\frac{\Delta P_0}{P_0}\right)^2 + \left(\frac{\Delta P_C}{P_C}\right)^2}$$

Considering 3% random error and 1 cm thick cell: $\Delta\alpha_e = \frac{0.03\sqrt{2}}{L} = 4.2\ m^{-1}$

2) $\boldsymbol{\alpha_a \pm \Delta\alpha_a}$

Neglecting the errors on $\lambda, k,$ and dn/dT and following Eq. (6) [8]:

$$\alpha_a = \frac{1}{L} ln\left[\frac{P\ dn/dT}{P\ dn/dT - \lambda k\theta}\right]$$

It can be shown that: $\frac{\partial\alpha_{TL}}{\partial P} = -\frac{\lambda k\theta}{LP(Pdn/dT - \lambda k\theta)}$ and $\frac{\partial\alpha_a}{\partial\theta} = \frac{\lambda k}{L(Pdn/dT - \lambda k\theta)}$ resulting in:

$$\Delta\alpha_a = \frac{\lambda k}{L(P\ dn/dT - \lambda k\theta)}\sqrt{\left(-\frac{\theta}{P}\Delta P\right)^2 + (\Delta\theta)^2}$$

To determine the absolute random error $\Delta\theta$ one can estimate the error range $\theta_{max} - \theta_{min}$ in which it is reasonable to think the true value lies. Experimentally, it appeared to be unable to resolve a signal having less than $30\ mrad$, it would be logical to think that $\theta_{max} = \theta_{fit} + 30\ mrad$ and $\theta_{min} = \theta_{fit} - 30\ mrad$ where θ_{fit} is the value given by the fit of the acquired data. Then the probabilities show that $\Delta\theta \approx 2\sigma \approx 2\frac{60}{\sqrt{12}} = 35\ mrad$ with a 95% confidence interval.

3) $\boldsymbol{\Phi \pm \Delta\Phi}$

Leaving aside the corrective coefficient in Eq. (7) $\nu_i/\langle\nu_f\rangle$, the yield is given by:

$$\Phi = \left(\frac{e^{-\alpha_a L} - e^{-\alpha_e L}}{1 - e^{-\alpha_e L}}\right)$$

$$\Delta\Phi = \sqrt{\left(\frac{\partial\Phi}{\partial\alpha_a}\Delta\alpha_a\right)^2 + \left(\frac{\partial\Phi}{\partial\alpha_e}\Delta\alpha_e\right)^2}$$

Yet, $\frac{\partial\Phi}{\partial\alpha_a} = \frac{-Le^{-\alpha_a L}}{1-e^{-\alpha_e L}}$ and $\frac{\partial\Phi}{\partial\alpha_e} = Le^{-\alpha_e L}\frac{(1-e^{-\alpha_a L})}{(1-e^{-\alpha_e L})^2}$ resulting in:

$$\Delta\Phi = \sqrt{\left[\frac{-Le^{-\alpha_a L}}{(1-e^{-\alpha_e L})}\Delta\alpha_a\right]^2 + \left[Le^{-\alpha_e L}\frac{(1-e^{-\alpha_a L})}{(1-e^{-\alpha_e L})^2}\Delta\alpha_e\right]^2}$$

$$\Delta\Phi = \frac{L}{(1-e^{-\alpha_e L})}\sqrt{[e^{-\alpha_a L}\Delta\alpha_a]^2 + \left[e^{-\alpha_e L}\frac{(1-e^{-\alpha_a L})}{(1-e^{-\alpha_e L})}\Delta\alpha_e\right]^2}$$

By replacing $\Delta\alpha_a$ and $\Delta\alpha_e$ found here in 1) and 2), one can finally obtain:

$$\Delta\Phi = \frac{1}{(1-e^{-\alpha_e L})}\sqrt{\left[e^{-\alpha_a L}\frac{\lambda k}{(P\,dn/dT - \lambda k\theta)}\sqrt{\left(-\frac{\theta}{P}\Delta P\right)^2 + (\Delta\theta)^2}\right]^2 + \left[e^{-\alpha_e L}\frac{(1-e^{-\alpha_a L})}{(1-e^{-\alpha_e L})}\sqrt{\left(\frac{\Delta P_0}{P_0}\right)^2 + \left(\frac{\Delta P_C}{P_C}\right)^2}\right]^2}$$

Appendix 2

Here we measure α_a using least squares regression analysis. Using Eq. (5), θ_{eff} defined in Eq. (2) is measured as a function of varying P to obtain the slope of the linear regression line as shown in Fig. A-1:

$$m = \frac{\theta_{eff}}{P} = \frac{dn/dT}{\lambda k}[1 - exp(-\alpha_a L)]$$

by isolating α_a in this expression:

$$\alpha_a = \frac{1}{L} ln\left[\frac{dn/dT}{dn/dT - \lambda k m}\right] \qquad \text{(A2-1)}$$

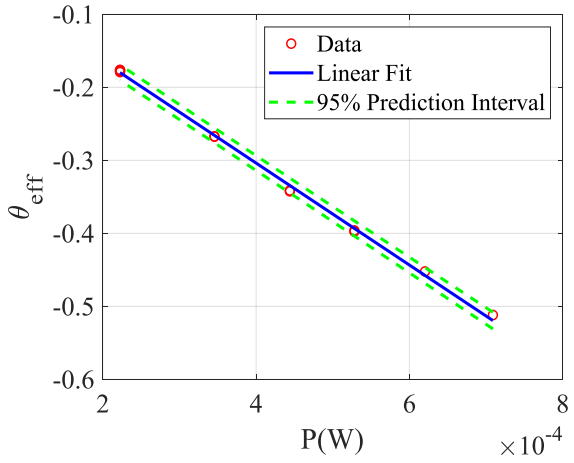

Fig. A-1: Linear fit of data with 95% prediction interval using cresyl violet solution in methanol ($\alpha_e(m^{-1}) = 48.15$).

The estimation of α_a and $\Delta\alpha_a$ are obtained using two Matlab functions: i) $[m, S] = polyfit(P, \theta_{eff}, 1)$ to evaluate the first-degree polynomial fit in m at the points in P; ii) $[\theta_{eff,\text{fit}}, \Delta m] = Polyval(m, P, S)$ to specify the error estimation structure S as the third input so that $polyval$ calculates an estimate of the standard error which is returned in Δm. This provides the slope of the least-squares line and displays the absolute error of this slope with a 95% confidence interval considering $2\Delta m$ (green lines in Fig. A-1). Then, Eq. A2-1 is derived to evaluate $\Delta\alpha_a = \lambda k \Delta m/[L(dn/dT - \lambda k m)]$. In the example shown here for cresyl violet, we have obtained: $\alpha_a = (22.3 \pm 0.2)\, m^{-1}$. Thus, knowing the extinction coefficient, $\alpha_e = (48 \pm 4) m^{-1}$, we can deduce the quantum yield Φ according to Eq. (7). Finally, taking into account the calculation detailed in section 3 of Appendix 1, we obtain $\Delta\Phi$. Hence $\Phi(\%) = 56 \pm 2$.

References

1 H. Cabrera, F. Matroodi, H. D. Cabrera-Díaz, and E. E. Ramírez-Miquet, "Frequency-resolved photothermal lens: An alternative approach for thermal diffusivity measurements in weak absorbing thin samples," International Journal of Heat and Mass Transfer **158**, 120036 (2020).

2 Z. Safi Keykeleh, E. Mohammadi-Manesh, and M. R. Mohebbifar, "Investigation of the effect of temperature on opto-thermal parameters of glycerol and ethylene glycol using laser thermal lens spectroscopy," Optical and Quantum Electronics **55**, 833 (2023).

3 H. A. Badran, "Thermal properties of a new dye compound measured by thermal lens effect and Z-scan technique," Applied Physics B **119**, 319-326 (2015).

4 C. Estupiñán-López, C. T. Dominguez, and R. E. de Araujo, "Eclipsing thermal lens spectroscopy for fluorescence quantum yield measurement," Optics express **21**, 18592-18601 (2013).

5 M. R. Mohebbifar, "Investigation of thermal lens performance of rhodamine 6G and rhodamine B at different concentration using pump/probe laser thermal lens spectroscopy," Optik **242**, 166902 (2021).

6 H. Cabrera, J. Akbar, D. Korte, E. E. Ramírez-Miquet, E. Marín, J. Niemela, Z. Ebrahimpour, K. Mannatunga, and M. Franko, "Trace detection and photothermal spectral characterization by a tuneable thermal lens spectrometer with white-light excitation," Talanta **183**, 158-163 (2018).

7 R. C. C. Leite, R. S. Moore, and J. R. Whinnery, "Low absorption measurements by means of the thermal lens effect using an He–Ne laser," Applied Physics Letters **5**, 141-143 (1964).

8 A. Marcano, C. Loper, and N. Melikechi, "Pump–probe mode-mismatched thermal-lens Z scan," JOSA B **19**, 119-124 (2002).

9 A. Marcano, C. Loper, and N. Melikechi, "High-sensitivity absorption measurement in water and glass samples using a mode-mismatched pump-probe thermal lens method," Applied Physics Letters, **78**, 3415-3417 (2001).

10 V. Besse, G. Boudebs, and H. Leblond, "Determination of the third-and fifth-order optical nonlinearities: the general case," Applied Physics B **116**, 911-917 (2014).
11 E. L. Falcão-Filho, C. B. de Araújo, C. A. C. Bosco, L. H. Acioli, G. Poirier, Y. Messaddeq, G. Boudebs, and M. Poulain, "Nonlinear optical properties of tungstate fluorophosphate glasses," Journal of applied physics **96**, 2525-2529 (2004).
12 N. Vermeulen, D. Espinosa, A. Ball et al, "Post-2000 nonlinear optical materials and measurements: Data tables and best practices," Journal of Physics: Photonics **5**, 035001 (2023).
13 C. B. De Araújo, A. S. L Gomes, and G. Boudebs, "Techniques for nonlinear optical characterization of materials: a review," Reports on Progress in Physics **79**, 036401 (2016).
14 C. Hu, and J. R. Whinnery, "New thermooptical measurement method and a comparison with other methods," Applied Optics **12**, 72-79 (1973).
15 C. Würth, M. Grabolle, J. Pauli, M. Spieles, and U. Resch-Genger, "Relative and absolute determination of fluorescence quantum yields of transparent samples," Nature protocols **8,** 1535-1550 (2013).
16 C. Würth, M. Grabolle, J. Pauli, M. Spieles, and U. Resch-Genger, "Comparison of methods and achievable uncertainties for the relative and absolute measurement of photoluminescence quantum yields," Analytical chemistry**83**, 3431-3439 (2011).
17 C. Würth, M. G. González, R.Niessner, U. Panne, C. Haisch, and U. Resch-Genger, "Determination of the absolute fluorescence quantum yield of rhodamine 6G with optical and photoacoustic methods–Providing the basis for fluorescence quantum yield standards," Talanta **90**, 30-37 (2012).
18 S. Vavilov, "The fluorescence efficiency of dye solutions." Z Phys **22**, 266-272 (1924).
19 C. A. Parker, and W. T. Rees, "Correction of fluorescence spectra and measurement of fluorescence quantum efficiency," Analyst **85**, 587-600 (1960).
20 K. Rurack, *Fluorescence quantum yields: methods of determination and standards* (Standardization and quality assurance in fluorescence measurements I: techniques, 2008)
21 S. Fery-Forgues, and D. Lavabre. "Are fluorescence quantum yields so tricky to measure? A demonstration using familiar stationery products," Journal of chemical education **76**, 1260 (1999).
22 C. Jacinto, et al, "Thermal lens and Z-scan measurements: Thermal and optical properties of laser glasses–A review." Journal of Non-Crystalline Solids 352(32-35), 3582-3597 (2006).
23 J-B. Zinoune, C. Cassagne, M. H. V. Werts, M. Loumaigne, M. Chis, and G. Boudebs, "Wavelength-dependence of the photothermal efficiency of gold nanoparticles in solution by Z-scan photothermal lens spectroscopy," Chemical Physics Letters **823**, 140501 (2023).
24 C. B. De Araújo, A. Humeau, G. Boudebs, V. D. Del Cacho, and L. R. P Kassab, "Giant third-order nonlinearity of lead and germanium based films in the visible and in the infrared," Journal of applied physics **101**, (2007).
25 K. Fedus, G. Boudebs, Q. Coulombier, J. Troles, and X. H. Zhang, "Nonlinear characterization of GeS2–Sb2S3–CsI glass system," Journal of Applied Physics **107**, (2010).
26 O. Ba, M. Chis, C. Cassagne, and G. Boudebs, "Phase shift imaging in thin films using CW Z-scan based technique," Physica B: Condensed Matter **603**, 412608 (2021).
27 D. Manzani, C. B. De Araújo, G. Boudebs, Y. Messaddeq, and S. J. L. Ribeiro, "The role of Bi2O3 on the thermal, structural, and optical properties of tungsten-phosphate glasses," The Journal of Physical Chemistry B **117**, 408-414 (2013).
28 I. Angert, S. R. Karuka, J. Kohler, Y. Chen, and J. D. Mueller, "The Reliability of Fluorescence Z-Scan Analysis in the Complex Environment of the Living Cell," Biophysical Journal **120**, 183 (2021).
29 G. Boudebs, and S. Cherukulappurath, "Nonlinear refraction measurements in presence of nonlinear absorption using phase object in a 4f system," Optics communications **250**, 416-420 (2005).
30 G. Boudebs, M. Chis, and A. Monteil, "Contrast increasing by third-order nonlinear image processing: a numerical study for microscopic rectangular objects," Optics communications **150**, 287-296 (1998).
31 G. Boudebs, and C. B. De Araújo, "Characterization of light-induced modification of the nonlinear refractive index using a one-laser-shot nonlinear imaging technique," Applied physics letters **85**, 3740-3742 (2004).
32 R. A. Cruz, V. Pilla, and T. Catunda. "Quantum yield excitation spectrum (UV-visible) of CdSe/ZnS core-shell quantum dots by thermal lens spectrometry," Journal of Applied Physics **107** (2010).
33 R. A. Cruz, T. Catunda, W. M. Facchinatto, D. T. Balogh, and R. M. Faria, "Absolute photoluminescence quantum efficiency of P3HT/CHCl3 solution by Thermal Lens Spectrometry," Synthetic metals **163**, 38-41 (2013).
34 C. Würth, D. Geißler, T. Behnke, M. Kaiser, and U. Resch-Genger, "Critical review of the determination of photoluminescence quantum yields of luminescent reporters," Analytical and bioanalytical chemistry **407**, 59-78 (2015).
35 C. Cassagne, O. Ba, and G. Boudebs, "Time-Resolved cw Thermal Z-scan for Nanoparticles Scattering Evaluation in Liquid Suspension," Materials **15**, 5008 (2022).
36 S. J. Sheldon, L. V. Knight, and J. M. Thorne, "Laser-induced thermal lens effect: a new theoretical model," Applied optics **21**, 1663-1669 (1982).
37 C. A. Carter, and J. M. Harris, "Comparison of models describing the thermal lens effect," Applied optics **23**, 476-481 (1984).

38 https://www.ophiropt.com/mam/celum/celum_assets/op/resources/PD300-UV_PD300-UV-193_PD300-IR_PD300-IRG.pdf?0
39 https://www.sigmaaldrich.com/FR/fr/product/sigma/83689
40 R. A. Velapoldi, and H. H. Tønnesen, "Corrected emission spectra and quantum yields for a series of fluorescent compounds in the visible spectral region," Journal of fluorescence **14**, 465-472 (2004).
41 https://www.ophiropt.com/laser--measurement/knowledge-center/article/1110
42 Consisting of discrete [Co(OH2)6]2+ and [NO3]− ions dissolved in methanol. https://www.sigmaaldrich.com/FR/fr/substance/cobaltiinitratehexahydrate2910310026229
43 https://www.sigmaaldrich.com/FR/fr/product/sigald/34860
44 https://www.sigmaaldrich.com/FR/fr/product/sial/p7632
45 https://www.sigmaaldrich.com/FR/fr/product/aldrich/255246
46 S. J. Isak, and E. M. Eyring, "Fluorescence quantum yield of cresyl violet in methanol and water as a function of concentration," The Journal of Physical Chemistry **96**, 1738-1742 (1992).
47 D. Magde, J. H. Brannon, T. L. Cremers, and J. Olmsted, "Absolute luminescence yield of cresyl violet. A standard for the red," Journal of Physical Chemistry **83**, 696-699 (1979).
48 K. H. Drexhage, *Structure and properties of laser dyes* (Dye lasers, 2005).
49 D. Magde, R. Wong, and P. G. Seybold, "Fluorescence quantum yields and their relation to lifetimes of rhodamine 6G and fluorescein in nine solvents: Improved absolute standards for quantum yields," Photochemistry and photobiology **75**, 327-334 (2002).
50 S. Mertens, B. Siegmund, and K. Vandewal, "Ultra-precise photothermal measurements reveal near unity photoluminescence quantum yields of molecular emitters in solution," Materials Horizons **10**, 594-600 (2023).
51 R. F. Kubin, and A. N. Fletcher, "Fluorescence quantum yields of some rhodamine dyes," Journal of Luminescence **27**, 455-462 (1982).
52 https://www.sigmaaldrich.com/FR/fr/product/sigma/83697
53 M. J. Snare, F. E. Treloar, K. P. Ghiggino, and P. J. Thistlethwaite, "The photophysics of rhodamine B," Journal of Photochemistry **18**, 335-346 (1982).
54 J. H. Brannon, and D. Magde, "Absolute quantum yield determination by thermal blooming. Fluorescein," The Journal of Physical Chemistry **82**, 705-709 (1978).